Available online at www.sciencedirect.com
SCIENCE DIRECT®
Carbon 43 (2005) 1731–1742
CARBON
www.elsevier.com/locate/carbon

Raman microspectroscopy of soot and related carbonaceous materials: Spectral analysis and structural information

A. Sadezky [a,1], H. Muckenhuber [b], H. Grothe [b], R. Niessner [a], U. Pöschl [a,*]

[a] Institute of Hydrochemistry, Technical University of Munich, Marchioninistr. 17, D-81377 Munich, Germany
[b] Institute of Materials Chemistry, Vienna University of Technology, Veterinaerplatz 1/GA, A-1210 Vienna, Austria

Received 6 September 2004; accepted 10 February 2005
Available online 23 March 2005

Abstract

Experimental conditions and mathematical fitting procedures for the collection and analysis of Raman spectra of soot and related carbonaceous materials have been investigated and optimised with a Raman microscope system operated at three different laser excitation wavelengths (514, 633, and 780 nm). Several band combinations for spectral analysis have been tested, and a combination of four Lorentzian-shaped bands (G, D1, D2, D4) at about 1580, 1350, 1620, and 1200 cm^{-1}, respectively, with a Gaussian-shaped band (D3) at ~1500 cm^{-1} was best suited for the first-order spectra. The second-order spectra were best fitted with Lorentzian-shaped bands at about 2450, 2700, 2900, and 3100 cm^{-1}. Spectral parameters (band positions, full widths at half maximum, and intensity ratios) are reported for several types of industrial carbon black (Degussa Printex, Cabot Monarch), diesel soot (particulate matter from modern heavy duty vehicle and passenger car engine exhaust, NIST SRM1650), spark-discharge soot (Palas GfG100), and graphite. Several parameters, in particular the width of the D1 band at ~1350 cm^{-1}, provide structural information and allow to discriminate the sample materials, but the characterisation and distinction of different types of soot is limited by the experimental reproducibility of the spectra and the statistical uncertainties of curve fitting. The results are discussed and compared with X-ray diffraction measurements and earlier Raman spectroscopic studies of comparable materials, where different measurement and fitting procedures had been applied.

Keywords: Soot, Graphitic carbon; Raman spectroscopy; Microstructure

1. Introduction

Soot is technically defined as the black solid product of incomplete combustion or pyrolysis of fossil fuels and other organic materials. It plays important roles as an industrial filler and pigment on the one hand (carbon black), and as a traffic-related air pollutant on the other hand (diesel soot). Soot is primarily composed of carbon (>80%) and consists of agglomerated primary particles with diameters on the order of 10–30 nm comprising crystalline and amorphous domains. The graphite-like crystalline domains typically consist of 3–4 turbostratically stacked graphene layers, with average lateral extensions (L_a) of up to ~3 nm and interlayer distances of about 3.5 Å, and can be regarded as highly disordered graphitic lattices [1,2]. In an ideal graphitic lattice the distance between parallel graphene layers (planar hexagonal structures of sp^2-hybridized carbon atoms with covalent bond lengths of 1.42 Å) is 3.35 Å, and the layers are arranged in an alternating sequence ABAB. This corresponds to a hexagonal closest crystal structure with unit cells of four C atoms at two types of lattice sites with different coordination (two or no neighbouring C atoms on a perpendicular axis through the adjacent

* Corresponding author. Tel.: +49 2180 78238; fax: +49 89 2180 78255.
E-mail address: ulrich.poeschl@ch.tum.de (U. Pöschl).
[1] Now at Laboratoire de Combustion et de Systemes Reactifs, CNRS, F-45071 Orleans, France.

0008-6223/$ - see front matter © 2005 Elsevier Ltd. All rights reserved.
doi:10.1016/j.carbon.2005.02.018

parallel layers). The amorphous (i.e. non-graphite-like) domains are composed of polycyclic aromatic compounds, which can be regarded as graphene layer precursors in irregular or onion-like arrangements (fullerenoid structures), and other organic and inorganic components (aliphatics, sulfate, metal oxides, etc.). The actual physical and chemical structure of soot, its elemental composition (carbon, hydrogen, oxygen, etc.), and the ratio of crystalline graphite-like to amorphous organic carbon depend on the starting materials and conditions of the combustion or pyrolysis process (fuel type, fuel/oxygen ratio, flame temperature, residence time, etc. [2,3]) The graphitic carbon fraction of soot can be increased by annealing procedures at high temperatures [2–5].

For the structural characterisation of highly ordered solid materials (crystalline long-range order) diffraction techniques are usually the methods of choice. For highly disordered materials such as soot, however, Raman spectroscopy is more promising, because it is sensitive not only to crystal structures but also to molecular structures (short-range order). The Raman signals of graphite crystals result from lattice vibrations and are very sensitive to the degree of structural disorder. The spectrum of near-ideal graphite, which is observed for large single graphitic crystals and highly oriented polycrystalline graphite (HOPG), significantly differs from the Raman spectra of disturbed graphitic lattices, such as regular polycrystalline graphite or boron-doted HOPG [6–17] (Table 1). Among the substances investigated in earlier studies are different types of graphite [6,12,13,17–19], diamond films [15,20], glassy carbon [18,19,21], amorphous and graphitic carbon films [4,22], coal, pitch and coal fibres [18], activated carbon [18,19], and fullerenes [23]. Rosen and Novakov [24,25] have first used Raman spectroscopy to prove the presence of graphite-like carbon in diesel engine soot, and their investigations have been followed up in several other studies [3,5,13,22,26,27]. Some of these studies found that different types of soot could be distinguished according to their degree of graphitisation [3,5,13,18,19,26]. In the acquisition, analysis, and interpretation of the broad and overlapping Raman bands of soot, however, a wide range of different approaches has been followed. The spectral parameters correlated to the degree of graphitisation have been determined in different ways, which makes the results hard to compare and limits their conclusiveness. Thus we have set out to investigate the applicability of Raman microspectroscopy for the structural characterisation of soot by systematic experiments and spectral analyses. Raman spectra have been recorded for a wide variety of soot and related materials (diesel soot, spark discharge soot, industrial carbon black, graphite, polycyclic aromatic hydrocarbons) under varying measurement conditions using a Raman microscope system with three different excitation wavelengths (λ_0). The Raman spectra have been analysed by curve fitting with different band combinations, and the obtained spectral parameters and their structural information are discussed in view of the results of earlier studies.

2. Experimental

2.1. Samples

Eight different types of industrial soot (carbon black) were available as powder samples (Degussa: S160, Printex 140U, Printex 25, Printex 60, Printex 75, Printex 90, and Printex XE2; Cabot: Monarch 77, Monarch 120). Spark discharge soot was taken from a glass flask at the outlet of a Palas GfG 1000 aerosol generator (powder sample).

Diesel soot was available as a standard reference material (SRM 1650, NIST; powder sample) and in the form of polycarbonate and glass fibre filter samples collected from the exhaust of modern diesel engines (A

Table 1
First-order Raman bands and vibration modes reported for soot and graphite (vs = very strong, s = strong, m = medium, w = weak)

Band[a]	Raman shift (cm^{-1})			Vibration mode[b]
	Soot	Disordered graphite[c]	Highly ordered graphite[d]	
G	~1580 cm^{-1}, s	~1580 cm^{-1}, s	~1580 cm^{-1}, s	Ideal graphitic lattice (E_{2g}-symmetry) [6,17]
D1 (D)	~1350 cm^{-1}, vs	~1350 cm^{-1}, m	–	Disordered graphitic lattice (graphene layer edges, A_{1g} symmetry) [6,17]
D2 (D′)	~1620 cm^{-1}, s	~1620 cm^{-1}, w	–	Disordered graphitic lattice (surface graphene layers, E_{2g}-symmetry) [17]
D3 (D″, A)	~1500 cm^{-1}, m	–	–	Amorphous carbon (Gaussian [26] or Lorentzian [3,18,27] line shape)
D4 (I)	~1200 cm^{-1}, w	–	–	Disordered graphitic lattice (A_{1g} symmetry) [10], polyenes [3,27], ionic impurities [18]

[a] Alternative band designations of earlier studies are given in brackets.
[b] Lorentzian line shape unless mentioned otherwise.
[c] Polycrystalline graphite (<100 nm) and boron-doted HOPG [17].
[d] Single graphitic crystals (>100 nm) and HOPG [17].

and B: heavy-duty vehicles; C and D: passenger cars). Graphite was investigated in the form of a solid electrode bar as used in the spark discharge generator (99.9995%, Johnston-Matthey) and in the form of powder samples (SHER graphite, <100 μm, Heraeus; synthetic graphite, 1–2 μm, Aldrich). The polycyclic aromatic hydrocarbon hexa-benzo-coronene (HBC) was synthesized and supplied by the research group of K. Müllen (Max Planck Institute for Polymer Research, Mainz, Germany).

2.2. X-ray diffraction

The investigated soot and graphite powder samples were placed on the sample support (silicon) of the X-ray diffractometer (Philips X'pert PW 3050/60) and illuminated with Ni-filtered copper radiation (Cu $K_{\alpha 1}$: $\lambda_1 = 1.54051$ Å; $K_{\alpha 2}$: $\lambda_2 = 1.54433$ Å). The diffraction pattern was recorded at room temperature in the 2Θ range from 10 to 60° (resolution 0.02°, counting time 5 s per interval).

2.3. Raman measurement and spectral analysis

The applied Raman microscope systems (Renishaw, System 2000; Yobin Yvon, LabRAM HR) consisted of a light microscope (Leica DL-LM; Olympus BX) coupled to a Raman spectrometer with three different excitation lasers. The microscope was equipped with four objectives with 5×, 20×, 50×, and 100× magnification, respectively, and with an eyepiece with 10× magnification. The microscope optics were used to focus the excitation laser beam onto the sample and to collect the backscattered light (180°). The Rayleigh scattering component was removed by a Notch filter, and the Raman-scattered light was dispersed by an optical grid and detected by a CCD camera (maximum sensitivity at 500–850 nm wavelength). The excitation lasers were an Ar ion laser ($\lambda_0 = 514$ nm, source power 17 mW), a He–Ne laser ($\lambda_0 = 632.8$ nm, source power 25 mW), and a NIR diode laser ($\lambda_0 = 780$ nm, source power 26 mW). The laser beam power was adjustable from 1% to 100% of the source power. The diameter of the laser spot on the sample surface was 1 μm for the fully focused laser beam, and 40 μm for the fully defocused laser beam at 50× objective magnification. The spectral resolution was about 6 cm^{-1} at 514 nm, 4 cm^{-1} at 633 nm, and 2 cm^{-1} at 780 nm. The instrument was calibrated against the Stokes Raman signal of pure Si at 520 cm^{-1} using a silicon wafer ((1 1 1) crystal plane surface). Instrument control and spectral analysis were performed with the software packages Renishaw WiRE (Renishaw) and GRAMS/32 (Galactic). For the powder samples, a dense layer of about one millimeter thickness was pressed with a steel spatula onto a silicon wafer (macroscopically smooth surface) and placed on the microscope sample holder; filter samples and the graphite bar were placed directly on the sample holder. The microscope was focused onto the sample surface using the white light source and the objective with 50× magnification. Then the white light was replaced by the laser beam and Raman spectra were recorded (Stokes Raman shift 500–4000 cm^{-1}). The Raman spectrometer was generally operated in the continuous scanning mode. The power of the excitation laser beam (1–100% relative intensity), spot diameter (0–100% defocusing), and exposure time have been varied to find optimum measurement conditions. For soot samples spectra of highest quality and reproducibility were generally obtained with fully defocused laser beam, laser beam powers of 10% (514 nm) to 100% (780 nm), and exposure times of at least 120 s. For graphite samples, on the other hand, best results were generally obtained with 100% of the laser source power and fully focused laser beam, and exposure times of at least 10 s. Depending on the sample type and excitation wavelength, modified measurement conditions also yielded high quality spectra (e.g. 100% laser power and 25% defocusing for soot with $\lambda_0 = 633$ nm).

Curve fitting for the determination of spectral parameters was performed with the software program GRAMS/32 (Galactic, Levenberg–Marquardt algorithm). The goodness-of-fit was indicated by the reduced χ^2 value, which would be unity for perfect agreement between the calculated fit curve and the observed spectrum. Values between 1 and 3 imply that the curve fit converges towards the observed spectrum; values larger than 3 indicate that the iteration has reached a minimum, but does not converge [28]. First- and second-order spectra were fitted separately without fixing or limiting the range of any spectral parameter in the iteration procedure. Different combinations of first-order Raman bands and

Table 2
Band combinations tested for curve fitting of first-order Raman spectra of soot in this work and in earlier studies (initial band positions; line shapes: L = Lorentzian, G = Gaussian)

Band	Initial position (cm^{-1})	(I) [18]	(II) [26]	(III)	(IV) [19]	(V) [3,27]	(VI)	(VII)	(VIII)	(IX)
G	1580	L	L	L	L	L	L	L	L	L
D1	1360	L	L	L	L	L	L	L	L	L
D2	1620	–	–	–	L	–	–	L	L	L
D3	1500	L	G	–	–	L	G	–	L	G
D4	1180	–	–	L	–	L	L	L	L	L

their initial positions tested in this study are listed in Table 2.

3. Results and discussion

3.1. X-ray diffractograms

The diffraction pattern of the synthetic graphite sample exhibits four distinctive narrow reflections in the 2Θ range 10–60°, which can be indicated as follows: 26.8° (002 layer), 42.3° (100), 44.5° (101) and 54.9° (102). In contrast, the investigated soot samples show only two broad reflections with intensity maxima at 24.9° and 43.6° (Printex XE2) and at 24.2° and 43.4° (Printex 90), respectively (Fig. 1).

In the diffractogram of Printex 90 an additional narrow signal appears at 42.9° (marked by *); this is not due to the carbonaceous material but can be attributed to a contamination with tungsten carbide. Curve fitting yields the full width at half maximum (FWHM) of these reflexes, and the *Debye-Scherrer* formula can be used to estimate the average size of the crystallites or graphite-like crystalline domains contained in the samples [29]. These were 250 nm for the synthetic graphite, 4 nm for Printex XE2, and only 2 nm for Printex 90. These values indicate a higher degree of order and graphitisation for Printex XE2 compared to Printex 90, which is consistent with the Raman spectroscopic results discussed below.

3.2. Raman spectra of graphite

The spectrum of the SHER graphite sample (Fig. 2) is characteristic of an undisturbed graphitic lattice and exhibits only one first-order band, the G ("Graphite") band at around 1580 cm^{-1} corresponding to an ideal graphitic lattice vibration mode with E_{2g} symmetry.

Such spectra are generally observed for highly oriented polycrystalline graphite (HOPG), and for single graphitic crystals, whose edge length L_a parallel to the graphene layers is larger than 100 nm. The spectrum of the graphite bar, on the other hand, exhibits additional first-order bands (D or "Defect" bands), which are known to be characteristic for disordered graphite and to grow in intensity relative to the G band with increasing degree of disorder in the graphitic structure. The most intensive of them is the D1 band, which appears at ~1360 cm^{-1} and corresponds to a graphitic lattice vibration mode with A_{1g} symmetry. Another first-order band accounting for structural disorder is the D2 band at ~1620 cm^{-1} which can be observed as a shoulder on the G band. Like the G band, the D2 band corresponds to a graphitic lattice mode with E_{2g} symmetry [9,10,18]. The relative intensities of both the D1 and D2 bands increased with increasing λ_0 (Fig. 3), which can be attributed to resonance effects [30].

Spectra similar to that of the graphite bar have been observed for HOPG doted with 0.5 mol% of boron [17]

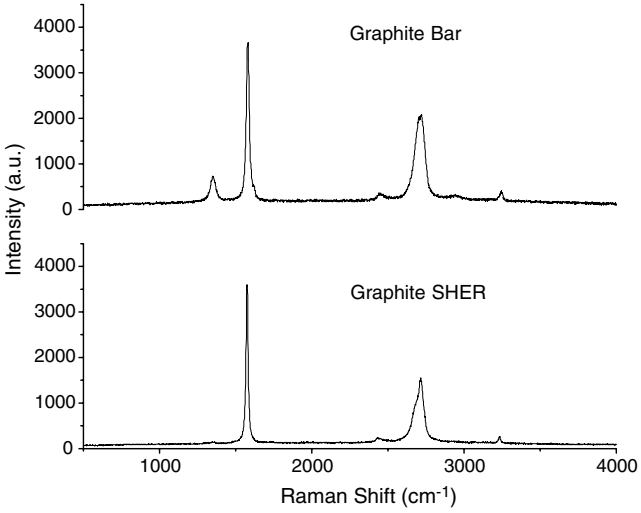

Fig. 2. Raman spectra of graphite samples with λ_0 = 514 nm.

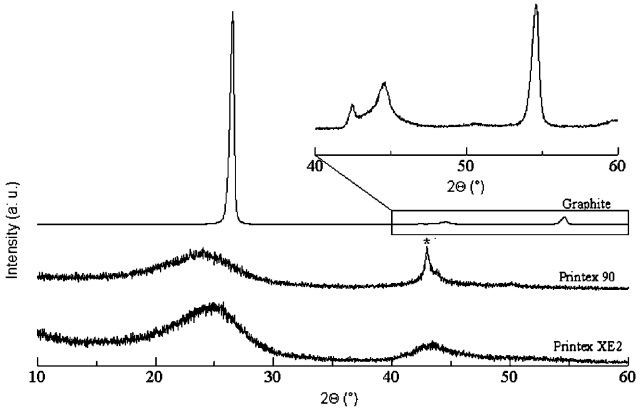

Fig. 1. X-ray diffractograms of graphite, Printex 90, and Printex XE2.

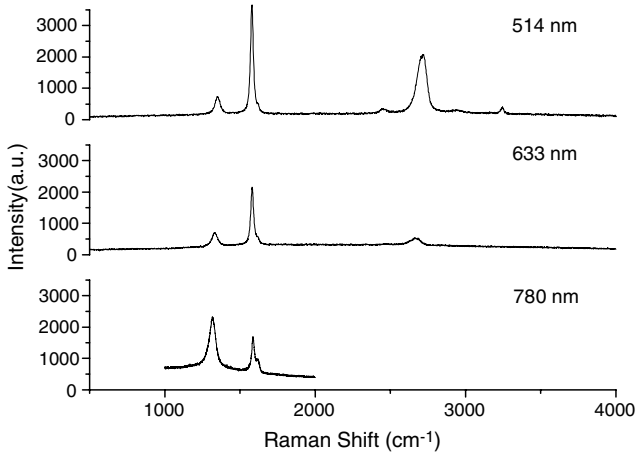

Fig. 3. Raman spectra of graphite bar with λ_0 = 514, 633, and 780 nm.

or polycrystalline graphites with L_a smaller than 1000 Å [6,8–16,21]. Theoretical calculations have shown that each of the first-order Raman bands visible in spectra of highly ordered and disordered graphites can be attributed to a vibrational mode of the ideal graphitic lattice [8,10]. For an ideal graphitic crystal (space group D^4_{6h} with unlimited translational symmetry) only a few of these vibrational modes are Raman active. In case of structural disorders, however, some ideally forbidden vibrational modes can become Raman active. The D1 band has been suggested to arise from graphene layer carbon atoms in immediate vicinity of a lattice disturbance like the edge of a graphene layer [14,17] or a heteroatom in case of doted graphite [17]. Moreover, this band has been observed in Raman spectra taken directly on the edge planes perpendicular to the graphene layers of large graphite single crystals and HOPG [14,17]. Thus, in polycrystalline carbonaceous materials consisting of large numbers of small graphitic crystallites carbon atoms at the edge of graphene layers are considered as the most probable origin of the D band [14,17]. The D2 band was assigned to a lattice vibration analogous to that of the G band but involving graphene layers at the surface of a graphitic crystal [31], i.e. graphene layers which are not directly sandwiched between two other graphene layers. Indeed, the D2 band was observed to replace the G band in intercalation compounds [9]. In polycrystalline graphitic materials it can be regarded as an indicator for the surface to volume ratio of graphitic crystals [19]. For both samples the Raman spectra recorded with $\lambda_0 = 514$ nm exhibited second-order bands at about 2450, 2720, and 3240 cm^{-1}. The band at 2720 cm^{-1} is the most intensive one and can be attributed to the first overtone of the D1 band, (2 * D1) [17,18]. The spectrum of the SHER graphite exhibits a split of the (2 * D1) band into a peak at ~2720 cm^{-1}, $(2 * D1)_1$, and a pronounced shoulder at ~2680 cm^{-1}, $(2 * D1)_2$. This split has been described before as a characteristic feature of undisturbed or highly ordered graphitic lattices [18]. The graphite bar exhibits no pronounced split but a relatively broad (2 * D1) band. Indeed all recorded second-order graphite spectra were best fitted with two rather than one Lorentzian-shaped (2 * D1) bands. The band at 3240 cm^{-1} can be assigned to the first overtone of the D2 band, (2 * D2) [17]. The band at 2450 cm^{-1} can be attributed to the Raman-active first overtone of a Raman-inactive graphitic lattice vibration mode at ~1220 cm^{-1} [10,17,32]. We denominate it (2 * D4) in analogy to first and second-order bands of soot with similar Raman shift.

For the graphite bar an additional higher-order band is observed at 2950 cm^{-1}, which has been assigned to a combination of the G and D modes characteristic for disturbed graphitic structures, (G + D) [17,18]. All observed second-order Raman bands can be attributed to overtones and combinations of known lattice vibration modes. Upon spectral analysis all signals except the very weak (G + D) band could be fitted with Lorentzian-shaped bands and χ^2 values below 2.

3.3. Raman spectra of soot

Fig. 4 shows typical Raman spectra observed for different types of soot with $\lambda_0 = 514$ nm. The first-order spectra of soot generally exhibit two broad and strongly overlapping peaks with intensity maxima at ~1350 cm^{-1} and at ~1585 cm^{-1}. As discussed above and summarized in Table 1, the structure and Raman spectra of soot can be interpreted in terms of highly disordered graphitic structures. Accordingly, earlier studies have described the intensity maxima at ~1350 cm^{-1} and

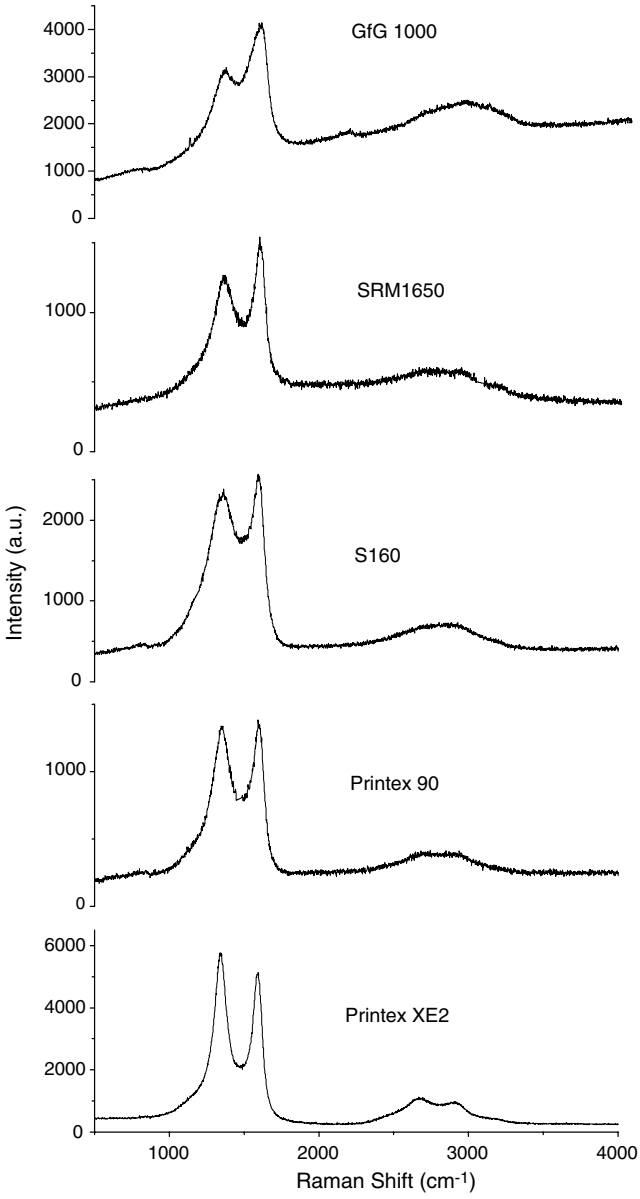

Fig. 4. Raman spectra of different types of soot with λ_0=514 nm.

~1585 cm^{-1} as D and G bands analogous to those of graphite [3,5,18,26]. Cuesta et al. [18], Jawhari et al. [26] and Sze et al. [19] suggested, that the peak at ~1585 cm^{-1} comprises not only the G but also the D2 band known from graphitic lattices, but only Sze et al. [19] included it in spectral analysis by curve fitting. The curve fitting results obtained in the present study and presented below clearly support the inclusion of the D2 band.

The high signal intensity between the two peak maxima can be attributed to another band at ~1500 cm^{-1}, which has been designated D3 band in a couple of earlier studies (Table 1). Cuesta et al. [18] and Jawhari et al. [26] suggested that the D3 band originates from the amorphous carbon fraction of soot (organic molecules, fragments or functional groups). Cuesta et al. [18] and Dippel et al. [3,27] assumed Lorentzian line shape for this band, whereas Jawhari et al. [26] proposed Gaussian line shape due to a statistical distribution of amorphous carbon on interstitial places in the disturbed graphitic lattice of soot. The spectral analyses presented below support the Gaussian line shape.

The peak at ~1350 cm^{-1} exhibits a shoulder at ~1200 cm^{-1}, which we denominate as D4 (Table 1). Dippel et al. [3,27] observed this band at ~1190 cm^{-1} in Raman spectra of flame soot and tentatively attributed it to sp^2-sp^3 bonds or C–C and C=C stretching vibrations of polyene-like structures. Sze et al. [19] observed a similar feature for glassy carbon, but did not include it in the spectral analysis by curve fitting. The curve fitting results obtained in the present study and presented below support the inclusion of a D4 band with Lorentzian line shape at ~1180 cm^{-1} in the Raman spectra of all investigated types of soot.

In some soot spectra very small peaks could be observed at ~900 cm^{-1} (Fig. 4, GfG1000, Printex 90, S 160). Such signals have not yet been reported for soot, but they might correspond to very weak bands reported by Wang et al. [17] for boron-doted HOPG (A_{1u} vibration mode of graphitic lattice). Due to their very low intensity and irregular occurrence, these signals were not taken into account in the spectral analyses presented below.

In the Raman spectra recorded with λ_0 = 514 nm all soot samples exhibited broad signals in the range of about 2300 cm^{-1} to 3300 cm^{-1} (Fig. 4). According to Cuesta et al. [18] these can be attributed to second-order bands, i.e. overtones and combinations of graphitic lattice vibration modes. The two pronounced peaks at ~2700 cm^{-1} and 2900 cm^{-1} have been assigned to the (2 * D) overtone and (G + D) combination, respectively. Additional shoulders at ~3100 cm^{-1} and ~2400 cm^{-1} can be assigned to the (2 * D2) and (2 * D4) overtones, respectively. This interpretation is consistent with the results of earlier studies [18] and with the spectral analyses by curve fitting presented below. With λ_0 = 633 nm the second-order signals were less pronounced, and with λ_0 = 780 nm they could not be observed at all.

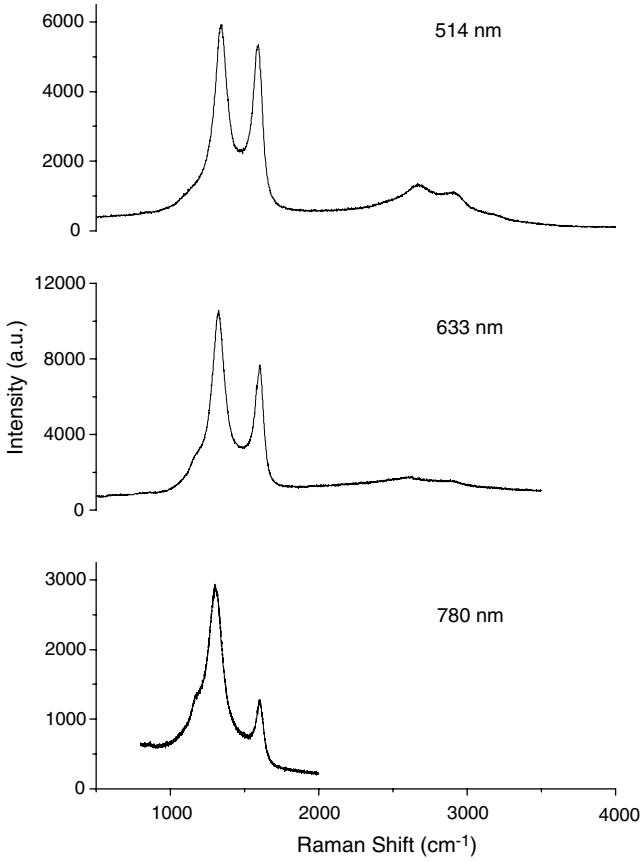

Fig. 5. Raman spectra of Printex XE2 with λ_0=514, 633, and 780 nm.

Fig. 5 shows the Raman spectra of Printex XE2 soot measured with λ_0 = 514, 633, and 780 nm. The change of relative signal intensities with excitation wavelength is consistent with earlier studies, can be attributed to resonance effects, and will be discussed below [11,13,17,30].

Fig. 6 shows the Raman spectrum of the polycyclic aromatic hydrocarbon (PAH) hexabenzocoronene

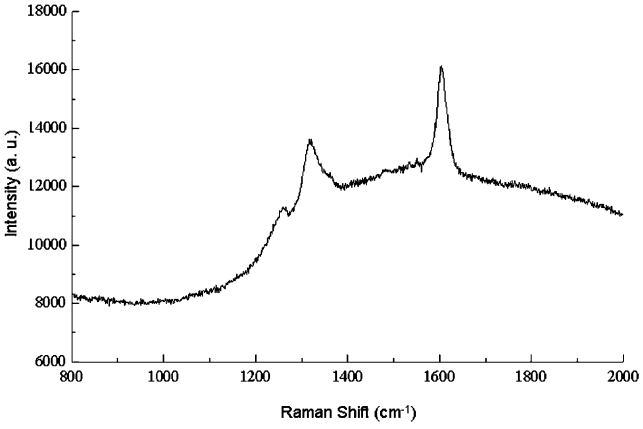

Fig. 6. Raman spectrum of hexabenzocoronene (HBC) with λ_0=633 nm.

(HBC), which can be regarded as a graphene layer section with lateral extensions of about 1.5 nm and thus as a model for the building blocks of small graphitic domains in soot. Indeed the main peaks occur at similar positions as in the spectra of soot: G band at $\sim$1600 cm^{-1} and D band at $\sim$1320 cm^{-1}. The peak at $\sim$1250 cm^{-1}, however, is more pronounced than the comparable D4 band, whereas HBC exhibits no significant D3 band. The observations are in good agreement with theoretical calculations for the vibration modes of HBC and other PAH [33].

3.4. Spectral analysis by curve fitting

For the analysis and determination of spectral parameters by curve fitting nine different combinations of first-order Raman bands have been tested. These band combinations are summarised in Table 2 with the applied line shapes (Lorentzian or Gaussian) and initial band positions. Most earlier analyses of soot Raman spectra have considered only three bands: G, D (comprising D1 and neighbouring bands), and either D′ (D2) or D″ (D3, Table 1). Here we present the first systematic inter-comparison of these earlier approaches with a new approach including all reported first-order Raman bands of soot (G and D1–D4, Table 1). The goodness-of-fit achieved with the different band combinations is indicated by the reduced χ^2 values summarized in Table 3.

For all investigated soot samples and excitation wavelengths the best results, i.e. the lowest χ^2 values were obtained with combination (IX), which includes the Lorentzian-shaped bands G, D1, D2, and D4 and the Gaussian-shaped band D3. Exemplary curve fits are illustrated in Fig. 7 for SRM 1650 diesel soot and Printex XE2. In most cases the second-best results were obtained with combination (VIII) consisting of five Lorentzian-shaped bands, while the combinations consisting of fewer bands yielded substantially higher χ^2 values. On the other hand, test calculations including an additional, hypothetical sixth band did not lead to a significant reduction of χ^2 compared to the fitting results obtained with five bands.

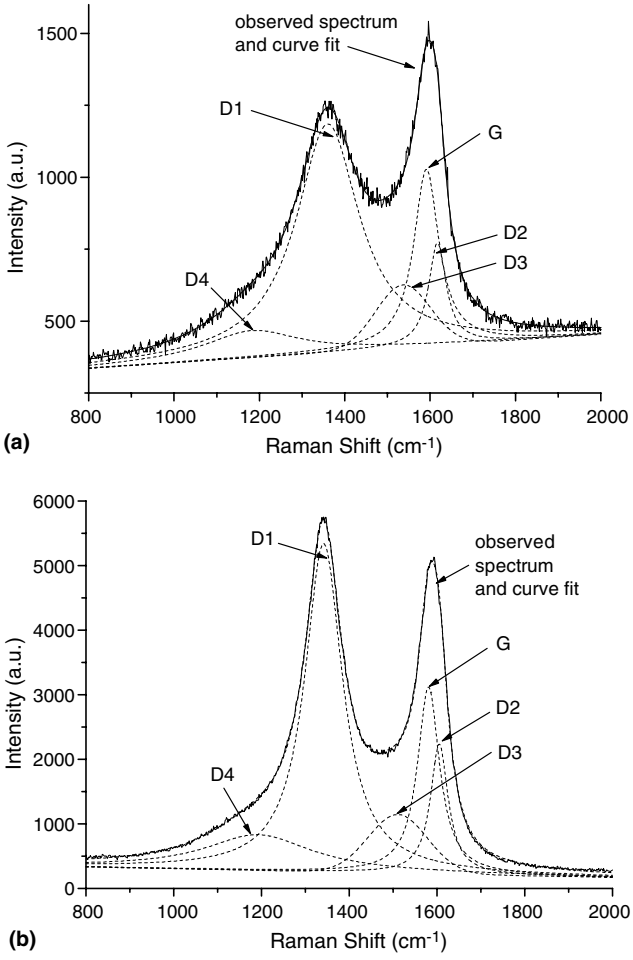

Fig. 7. Curve fit with band combination (IX) for the first-order Raman spectra (λ_0 = at 514 nm) of diesel soot SRM1650 (a) and Printex XE2 (b).

To corroborate these findings, multiple spectra have been recorded under identical experimental conditions

Table 3
Goodness-of–fit for the Raman spectra of exemplary soot samples obtained with different band combinations (Table 2) and indicated by reduced χ^2 values (χ^2 = 1 ideal fit; χ^2 < 3 convergence; χ^2 > 3 minimum without convergence)

Sample	λ_0	(I)	(II)	(III)	(IV)	(V)	(VI)	(VII)	(VIII)	(IX)
SRM 1650	514	2.46	2.02	11.49	12.62	1.77	1.41	2.46	1.25	1.12
Printex XE2	514	23.32	19.89	16.73	23.32	7.22	4.28	9.68	2.99	1.58
Printex XE2	633	9.05	7.94	11.81	9.05	3.71	2.67	3.71	2.34	1.66
Diesel A[a]	633	9.57	7.20	13.73	19.65	1.95	2.11	7.21	1.33	1.24
Diesel B[a]	633					1.77	1.49		1.34	1.28
Diesel C[a]	633					1.71	1.90		1.60	1.51
Monarch 77[b]	633	6.70	4.49	6.70	6.70	1.96	3.95	6.26	1.62	1.32
Monarch 120[a]	633					1.58	2.93		1.33	1.18
GfG 1000[c]	633	6.96	5.73	18.60	20.82	2.68	2.46	6.98	1.93	1.53

[a] 6 spectra.
[b] 12 spectra.
[c] 11 spectra.

(λ_0 = 633 nm, 100% laser power, 25% defocusing) for six different soot samples (Table 3, superscripts a–c). Averaging over the 47 spectra yields $\chi^2 = 1.3 \pm 0.2$ for band combination (IX), $\chi^2 = 1.6 \pm 0.3$ for combination (VIII), $\chi^2 = 2.5 \pm 0.5$ for combination (VI), and $\chi^2 = 2.0 \pm 0.5$ for combination (V) which had been applied by Dippel et al. [3,27]. All other combinations, including those applied by Cuesta et al. [18], Jawhari et al. [26], and Sze et al. [19] yielded average χ^2 values substantially higher than 3 (minimum but no convergence of Levenberg–Marquardt fit algorithm).

The results clearly indicate that all five bands (G, D1, D2, D3, D4) should be taken into account for a complete analysis and interpretation of soot Raman spectra in the range of 1200–1600 cm^{-1}, and that the shape of the D3 band is indeed Gaussian rather than Lorentzian. The second-order bands of the recorded soot spectra were best fitted with a combination of four Lorentzian-shaped bands with their initial positions at 2450, 2700, 2900, and 3100 cm^{-1}, yielding reduced χ^2 values lower than 2. Exemplary curve fits are illustrated in Fig. 8 for SRM 1650 diesel soot and Printex XE2.

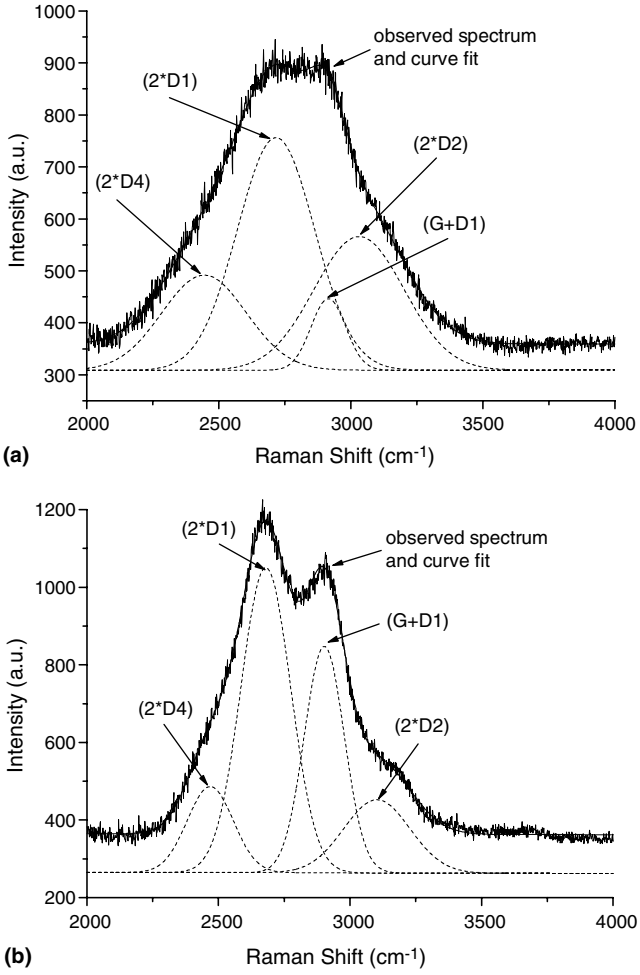

Fig. 8. Curve fits for the second-order Raman spectra (λ_0 = 514 nm) of diesel soot SRM 1650 (a) and Printex XE2 (b).

3.5. Band parameters

For all investigated soot and graphite samples spectral parameters have been determined by curve fitting with band combination (IX). The complete data set with mean values and standard deviations of first-order band positions (Raman shift), full widths at half maximum (FWHM), and intensity (peak area) ratios is given in the electronic supplement (up to 12 spectra per sample; Tables S1–S3 with λ_0 = 514, 633, and 780 nm, respectively). Characteristic features will be outlined below.

The mean values of the G band positions (Stokes Raman shift) observed for different types of soot and graphite ranged from 1571 cm^{-1} to 1598 cm^{-1} with standard deviations (s.d.) up to 18 cm^{-1}, without significant dependencies on λ_0 or significant differences between soot and graphite. The mean values of the G band FWHM observed for different types of soot ranged from 46 cm^{-1} to 101 cm^{-1} (s.d. $\leqslant$30 cm^{-1}). Significantly lower values were observed for graphite: 20–22 cm^{-1} (s.d. $\leqslant$4 cm^{-1}) for the graphite bar and 15–16 cm^{-1} (s.d. $\leqslant$3 cm^{-1}) for the highly-ordered SHER graphite.

The D1 band position exhibited a pronounced dependence on the laser excitation wavelength, with mean values of 1301–1317 cm^{-1} (s.d. $\leqslant$2 cm^{-1}) for λ_0 = 780 nm, 1323–1339 cm^{-1} (s.d. $\leqslant$8 cm^{-1}) for λ_0 = 633 nm, and 1343–1358 cm^{-1} (s.d. $\leqslant$8 cm^{-1}) for λ_0 = 514 nm, without significant difference between graphite bar and different types of soot. The D1 band FWHM were significantly lower for the graphite bar (42–49 cm^{-1}, s.d. $\leqslant$7 cm^{-1}) and for Printex XE2 soot (101–116 cm^{-1}, s.d. $\leqslant$5 cm^{-1}) than for all other investigated types of soot (157–227 cm^{-1}, s.d. $\leqslant$ 15 cm^{-1}), as will be discussed below. In contrast to the band position, however, the FWHM exhibited no systematic dependence on λ_0. The D1/G band intensity (peak area) ratios, I_{D1}/I_G, generally increased with the excitation wave length. For the graphite bar I_{D1}/I_G increased from 0.2 (s.d. 0.1) at λ_0 = 514 and 0.4 (s.d. 0.3) at 633 nm to 2.7 (s.d. 1.0) at 780 nm. For the different types of soot I_{D1}/I_G was highly variable and increased from 3.0 to 9.1 (s.d. $\leqslant$ 3) at λ_0 = 514 nm and 3.3–10.5 (s.d. $\leqslant$2.7) at 633 nm to 9.1–21.7 (s.d. $\leqslant$ 1.9) at 780 nm. The dependency of D1 band position and intensity on laser excitation wavelength is consistent with earlier studies and can be attributed to resonance effects [11,13,17,30]. The mean values of the D2 band position ranged from 1599 cm^{-1} to 1624 cm^{-1} (s.d. $\leqslant$ 12 cm^{-1}). The D2 band FWHM were significantly lower for the graphite bar (13–22 cm^{-1}, s.d. $\leqslant$7 cm^{-1}) than for soot (31–72 cm^{-1}, s.d. $\leqslant$ 14 cm^{-1}). For the graphite bar I_{D2}/I_G increased from 0.02 (s.d. 0.01) at λ_0 = 514 and 0.07 (s.d. 0.04) at 633 nm to 0.2 (s.d. 0.05) at 780 nm. For the different types of soot I_{D2}/I_G varied in the range of 0.3–1.4 (s.d. $\leqslant$ 0.9) and exhibited no systematic increase with λ_0. The D3 and D4 bands were observed for soot only.

The mean values of the D3 band position ranged from 1489 cm^{-1} to 1545 cm^{-1} (s.d. $\leqslant$32 cm^{-1}); the FWHM varied in the range of 110–206 cm^{-1} (s.d. $\leqslant$65 cm^{-1}). I_{D3}/I_G varied in the range of 0.3–2.1 (s.d. $\leqslant$ 0.8). The mean values of the D4 band position ranged from 1127 cm^{-1} to 1208 cm^{-1} (s.d. $\leqslant$ 109 cm^{-1}) with FWHM in the range of 144–311 cm^{-1} (s.d. $\leqslant$ 150 cm^{-1}). I_{D4}/I_G varied in the range of 0.2–1.5 (s.d. $\leqslant$0.7) at λ_0 = 514 and 633 nm, and it increased to 1.7–9.7 (s.d. $\leqslant$ 1.4) at 780 nm. The observed increase is consistent with the fact that earlier Raman studies of soot performed with λ_0 = 514 nm have not reported a band at ~1200 cm^{-1}, whereas Dippel et al. [3,27] observed a strong D4 band in the Raman spectra of flame soot recorded with λ_0 = 1064 nm.

3.6. Reproducibility of spectra and spectral parameters

Beyssac et al. [34] reported that the structural heterogeneity of carbonaceous materials like natural coal, cokes and anthracite limited the applicability of Raman microspectroscopy for their characterisation. The spectra they recorded with conventional Raman microspectroscopy at different positions on the sample looked very different, reflecting the heterogeneity of the material. With Raman area mode microscopy probing large laser spots of about 40 μm diameter, on the other hand, they obtained well-reproducible average spectra of the investigated material.

With the Raman microscope and operating conditions applied in the present study, the diameter of the laser spot on the sample ranged between 1 μm (fully focused) and 40 μm (fully defocused). Since the diameters of primary particles of soot are only on the order of 10–30 nm, even the fully focused laser beam should probe at least several hundred primary particles. Therefore the recorded spectra should be fairly representative for the investigated samples, provided that the soot primary particles and agglomerates are well-mixed within the sample. Indeed the spectra recorded at different positions on the surface of a soot sample mostly looked very similar and could hardly be distinguished with the naked eye. Despite the very similar appearance of the spectra, however, the spectral parameters determined by curve fitting, in particular the signal intensity ratios, were highly variable. Exemplary spectra and fit curves for GfG1000 spark discharge soot are shown in Fig. 9.

They demonstrate that the deconvolution of the broad signal peaks into multiple bands by curve fitting is subject to high statistical uncertainty. The separation of the strongly overlapping G, D2, and D3 bands and the relative intensities of these bands appear to be particularly uncertain. For the spectra illustrated in Fig. 9 the intensity ratios varied as follows: I_{D1}/I_G 5.8–8.0, I_{D2}/I_G 0.6–1.0, I_{D3}/I_G 0.8–1.3. Similar variability has been observed for the other investigated types of soot and has

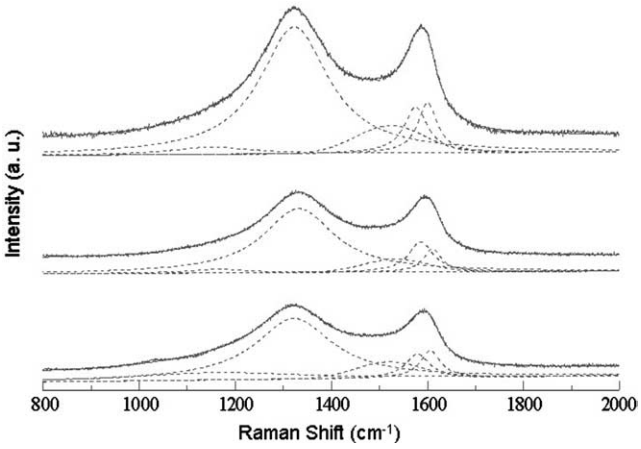

Fig. 9. Raman spectra recorded at different positions on a GfG1000 spark discharge soot sample (curve fits with band combination (IX)).

to be taken into account as a major source of uncertainty in the characterisation of soot by Raman spectroscopy. The uncertainties of curve fitting seem to be as important and limiting as the potential heterogeneity of soot samples. In any case high signal-to-noise ratios are a prerequisite for reliable curve fitting of soot Raman spectra. Up to now Raman-spectroscopic studies of soot reported little information about the reproducibility and statistical uncertainty of spectra and spectral fitting results. This should be a major aspect for future studies aimed at the characterisation and distinction of different types of soot. The measurement and data analysis methods reported in this and earlier studies have to be further refined and standardized to enable consistent and quantitative comparison and interpretation of spectral parameters from different samples and studies.

3.7. Structural information

Several earlier studies have reported that decreasing G and D band FWHM as well as decreasing D/G band intensity ratios indicated increasing degree of graphitisation of the investigated carbonaceous materials [3,5,6,12,17–19,26,27,35]. In most of these studies the "G band" was not separated from the D2 and D3 bands, and the "D band" included the D1 band as well as the D3 and D4 bands. Nevertheless, the results obtained in the present study with a refined fitting procedure and multiple D bands are consistent with the findings of earlier studies as far as the differences between highly ordered graphite (SHER), disordered graphite (bar), and soot are concerned. With respect to the distinction of different types of soot, however, G and D band FWHM were not found to be correlated with each other nor with signal intensity ratios.

For example, the Printex XE2 soot exhibited the lowest D1 and very low G band FWHM, which indicates that it has the highest degree of graphitisation among

all investigated types of soot and is consistent with the X-ray diffraction results reported above. The I_{D1}/I_G ratios of Printex XE2, however, were not generally lower than those of other investigated types of soot. At $\lambda_0 = 514$ nm the I_{D1}/I_G ratio of SRM1650 diesel soot was as low as that of Printex XE2 (Table S1) and at $\lambda_0 = 633$ nm several types of soot exhibited smaller I_{D1}/I_G ratios than Printex XE2 (Table S2). Only at $\lambda_0 = 780$ nm the I_{D1}/I_G ratio of Printex XE2 was clearly lower than those of all other investigated types of soot.

GfG1000 spark discharge soot, on the other hand, exhibited generally very high G and D1 band FWHM, which indicates that it has a particularly low degree of graphitisation and is consistent with earlier investigations by electron microscopy (prevalence of amorphous domains) and its relatively high chemical reactivity (rapid oxidation by oxygen and nitrogen oxides) [36,37]. The I_{D1}/I_G ratios of GfG1000, however, were not generally higher than those of other investigated types of soot. The G and D1 band FWHM of SRM1650 and other diesel soot samples ranged between those of GfG1000 and Printex XE2. The high statistical variability of the spectral parameters, however, did not enable unambiguous discrimination of the different diesel soot samples and various commercial carbon black materials.

Beyssac et al. [34] proposed to characterize the degree of organization of carbonaceous materials (natural coal, cokes and anthracite) by a parameter $R2 = I_{D1}/(I_G + I_{D1} + I_{D2})$, which they found to be less variable and statistically uncertain than the intensity ratios of individual bands. Indeed the R2 values calculated from the spectral parameters of soot samples investigated in the present study varied only between 0.5 and 0.8, but like the intensity ratios of individual bands they did not allow to distinguish different types of soot. Sze et al. [19] suggested that the I_{D2}/I_G ratio should be inversely proportional to the thickness of graphitic domains in soot. Indeed the I_{D2}/I_G ratio as well as the FWHM of the D2 band of the graphite bar were lower than those of the investigated soot samples (Tables S1–S3). Upon comparison of different types of soot, however, I_{D2}/I_G and the D2 band FWHM exhibited no significant correlation with each other nor with I_{D1}/I_G and the D1 band FWHM. The same applies for the spectral parameters of the D3 and D4 bands, which were observed for all investigated types of soot but not for graphite.

Earlier studies have reported an increase of I_{D3}/I_G with the proportion of amorphous carbon in soot [18,26]. This correlation, however, could not be generally confirmed in the present study. For example, I_{D3}/I_G at $\lambda_0 = 633$ nm was higher for the highly graphitised carbon black Printex XE2 (1.0 ± 0.3) than for the highly amorphous spark discharge soot GfG1000 and most diesel soot samples (0.3–0.8, Table S2). Sze et al. [19] observed higher Raman shifts for the D1 bands of diesel soot samples compared to industrial carbonaceous materials and attributed these to structural differences. For the peak at $\sim$1580 cm^{-1}, which comprises the G and D2 bands, Gruber et al. [5] reported a decrease of the Raman shift with increasing degree of graphitisation of the sample material. General trends of this kind, however, could not be observed and confirmed in the present study. Gruber et al. [5] also reported a change of relative signal intensities in the Raman spectra of carbon black heated upon heat treatment at 1300–3000 K (decrease of D and increase of G band), and they attributed this effect to a graphitisation of the sample material. The potential influence of heat treatment at lower temperatures on the structure and Raman spectra of soot was tested with gas soot Monarch 120 and GfG1000 spark discharge soot samples. These samples were heated to 1073 K for 10 h under vacuum, but the Raman spectra recorded before and after heat treatment (6 each) and the spectral parameters obtained by curve fitting exhibited no significant change. Nevertheless, further investigations of the evolution of Raman spectra upon heat treatment, desorption experiments, surface transformation, oxidation, and gasification of soot might help to elucidate soot particle surface and bulk properties, interactions, and transformations and are in preparation [38–42].

4. Conclusions

The spectral analyses by curve fitting with different band combinations provide quantitative evidence that all five reported first-order Raman bands of soot (G, D1, D2, D3, D4) have to be taken into account for a complete analysis and interpretation of the first-order spectral region (1000–2000 cm^{-1}), and that the shape of the D3 band is indeed Gaussian rather than Lorentzian. Unlike the band combinations applied in most earlier studies, this combination allowed to describe all measured spectra with excellent goodness-of-fit. The spectral parameters of several bands, especially the D1 band at $\sim$1350 cm^{-1}, exhibited a pronounced dependence on the excitation aser wavelength and allowed to distinguish different sample materials. The deconvolution of the broad signal peaks into multiple strongly overlapping bands is, however, subject to considerable statistical uncertainty, and the spectral parameters determined for very similar looking soot spectra were highly variable. Relative standard deviations ranged up to 30% for D1 band FWHM and up to 100% for the D1/G band intensity ratios. The range of parameter values measured for different types of soot were largely overlapping. Nevertheless, the D1 band FWHM enabled a clear and consistent distinction of Printex XE2 with particularly high degree of structural order (confirmed by X-ray diffraction) from all other investigated types of soot and for all applied excitation wavelengths (514, 633, and 780 nm). Neither the D1/G

band intensity ratio nor any other spectral parameter provided similarly clear information.

Overall, the results demonstrate that the characterisation and distinction of different types of soot by Raman microspectroscopy is feasible but limited by the reproducibility of spectra and statistical uncertainty of spectral parameters determined by curve fitting. The experimental and mathematical techniques applied in this and earlier studies should be further refined and standardized to enable consistent and quantitative comparison and interpretation of spectral parameters from different samples and measurements. In particular, the effects of sample characteristics and inhomogeneities on the one hand, and of the recording and fitting of Raman spectra on the other hand, have to be further clarified and separated. Comprehensive investigations with soot samples that are well characterized by complementary techniques like X-ray diffraction and (high resolution) electron microscopy are required to corroborate the rather vague and partly inconsistent structural interpretations of the Raman band parameters of soot reported in earlier studies and discussed above.

Acknowledgements

The authors thank K. Müllen and co-workers (Max-Planck Institute for Polymer Research, Mainz) as well as C. Adelhelm for providing hexabenzocoronene; D. Rothe for providing diesel soot samples; and H. Fink, N. Ivleva, and U. Panne for support with the Raman microscope. Financial support by the German Federal Ministry of Education and Research (AFO2000, CARBAERO, 07ATC05), the Max-Buchner-Forschungsstiftung (Project 2486), and the Vienna University of Technology is gratefully acknowledged.

Supplementary data

Supplementary data associated with this article can be found, in the online version, at doi:10.1016/j.carbon.2005.02.018.

References

[1] Homann KH. Fullerenes and soot formation—new pathways to large particles in flames. Angew Chem Int Ed 1998;37:2434–51.
[2] Lahaye J, Prado G. In: Thrower PA, editor. Chemistry and physics of carbon, vol. 14. New York: Decker; 1978. p. 14. 168.
[3] Dippel B, Heintzenberg J. Soot characterisation in atmospheric particles from different sources by NIR FT Raman spectroscopy. J Aerosol Sci 1999;30(Suppl. 1):907–8.
[4] Ramsteiner M, Wagner J. Resonant Raman scattering of hydrogenated amorphous carbon: evidence for π-bonded carbon clusters. Appl Phys Lett 1987;51:1355–7.
[5] Gruber T, Waldeck-Zerda T, Gerspacher M. Raman studies of heat-treated carbon blacks. Carbon 1994;32:1377–82.
[6] Tuinstra F, Koenig JL. Raman spectrum of graphite. J Chem Phys 1970;53:1126–30.
[7] Nakamizo M, Honda H, Inagaki M, Hishiyama Y. Raman spectra, effective Debye parameter and magnetoresistance of graphitized cokes. Carbon 1977;15:295–8.
[8] Nemanich RJ, Solin SA. First- and second-order Raman scattering from finite-size crystals of graphite. Phys Rev B 1979;20:392–401.
[9] Dresselhaus M, Dresselhaus SG. Intercalation compounds of graphite. Adv Phys 1981;30:290–8.
[10] Al-Jishi R, Dresselhaus G. Lattice-dynamical model for graphite. Phys Rev B 1982;26:4514–22.
[11] Vidano R, Fischbach DB, Willis L, Loehr TM. Observation of Raman band shifting with excitation wavelength for carbons and graphites. Solid State Commun 1981;39:341–4.
[12] Lespade P, Marchand A, Couzi M, Cruege F. Caractérisation de matériaux carbonés par microspectrométrie Raman. Carbon 1984;22:375–85.
[13] Mernagh TP, Cooney RP, Johnson RA. Raman spectra of graphon carbon black. Carbon 1984;22:39–42.
[14] Katagiri G, Ishida H, Ishitani A. Raman spectra of graphite edge planes. Carbon 1988;26:565–71.
[15] Knight DS, White WB. Characterisation of diamond films by Raman spectroscopy. J Mater Res 1989;4:385–93.
[16] Nikiel L, Jagodzinski PW. Raman spectroscopic characterisation of graphites: a reevaluation of spectra/structure correlation. Carbon 1993;31:1313–7.
[17] Wang Y, Alsmeyer DC, McCreery RL. Raman spectroscopy of carbon materials: structural basis of observed spectra. Chem Mater 1990;2:557–63.
[18] Cuesta A, Dhamelincourt P, Laureyns J, Martinez-Alonso A, Tascon JMD. Raman microprobe studies on carbon materials. Carbon 1994;32:1523–32.
[19] Sze SK, Siddique N, Sloan JJ, Escribano R. Raman spectroscopic characterisation of carbonaceous aerosol. Atmos Environ 2001;35:561–8.
[20] Wagner J, Ramsteiner M, Wild C, Koidl P. Resonant Raman scattering of amorphous carbon and polycrystalline diamond films. Phys Rev B 1989;40:1817–24.
[21] Nakamizo M, Kammereck R, Walker Jr PL. Laser Raman studies on carbons. Carbon 1974;12:259–67.
[22] Robertson J. Amorphous carbon. Adv Phys 1986;35:317–74.
[23] Garrell RL, Herne TM, Szafranski CA, Diederich F, Ettl F, Whetten RL. Surface-enhanced Raman spectroscopy of C_{60} on gold: evidence for symmetry reduction and perturbation of electronic structure in the adsorbed molecule. J Am Chem Soc 1991;113:6302–3.
[24] Rosen H, Novakov T. Raman scattering and the characterisation of atmospheric aerosol particles. Nature 1977;266:708–10.
[25] Rosen H, Novakov T. Identification of primary particulate carbon and sulfate species by Raman spectroscopy. Atmos Environ 1978;12:923–7.
[26] Jawhari T, Roid A, Casado J. Raman spectroscopic characterisation of some commercially available carbon black materials. Carbon 1995;33:1561–5.
[27] Dippel B, Jander H, Heintzenberg J. NIR FT Raman spectroscopic study of flame soot. Phys Chem Chem Phys 1999;1:4707–12.
[28] Galactic Industries Corporation. GRAMS/32 User's Guide V4.
[29] Warren BE. X-ray diffraction. Reading: Addison-Wesley; 1969.
[30] Matthews MJ, Pimenta MA, Dresselhaus G, Dresselhaus MS. Origin of dispersive effects of the Raman D band in carbon materials. Phys Rev B 1999;59:R6585–8.
[31] Dresselhaus MS, Dresselhaus G. Topics in applied physics, vol. 51. Berlin: Springer-Verlag; 1982. p. 3–57.

[32] Decius JC, Hexter RM. Molecular vibrations in crystals. New York: McGraw-Hill; 1977. p. 267–70.
[33] Mapelli C, Castiglioni C, Meroni E, Zerbi G. Graphite and graphitic compounds: vibrational spectra from oligomers to real materials. J Mol Struct 1999;480:615–20.
[34] Beyssac O, Goffé B, Petitet JP, Froigneux E, Moreau M, Rouzaud JN. On the characterization of disordered and heterogeneous carbonaceous materials by Raman spectroscopy. Spectrochim Acta Part A 2003;59:2267–76.
[35] Nakamura K, Fujitsuka M, Kitajima M. Disorder-induced line broadening in first-order Raman scattering from graphite. Phys Rev B 1990;41:12260–3.
[36] Messerer A, Rothe D, Pöschl U, Niessner R. Advances in the development of filterless soot deposition systems for the continuous removal or diesel particulate matter. Topics Catal 2004;30/31:247–50.
[37] Su DS, Jentoft R, Müller JO, Rothe D, Jacob E, Simpson CD, et al. Microstructure and oxidation behaviour of Euro IV diesel engine soot: a comparative study with synthetic model soot substances. Catal Today 2004;90:127–32.
[38] Pöschl U, Letzel T, Schauer C, Niessner R. Interaction of ozone and water vapor with spark discharge soot aerosol particles coated with benzo[*a*]pyrene: O_3 and H_2O adsorption, benzo[*a*]-pyrene degradation, and atmospheric implications. J Phys Chem A 2001;105:4029–41.
[39] Schauer C, Niessner R, Pöschl U. Analysis of nitrated polycyclic aromatic hydrocarbons by liquid chromatography with fluorescence and mass spectrometry detection: air particulate matter, soot, and reaction product studies. Anal Bioanal Chem 2004;378:725–36.
[40] Ammann M, Pöschl U, Rudich Y. Effects of reversible adsorption and Langmuir–Hinshelwood surface reactions on gas uptake by atmospheric particles. Phys Chem Chem Phys 2003;5:351–356.
[41] Pöschl U, Rudich Y, Ammann M. Kinetic model framework for aerosol and cloud surface chemistry and gas-particle interactions: Part 1—general equations, parameters, and terminology. Atmos Chem Phys, submitted for publication.
[42] Messerer A, Niessner R, Pöschl U. Comprehensive kinetic characterization of the oxidation and gasification of model and real diesel soot by nitrogen oxides and oxygen under engine exhaust conditions: measurement, Langmuir–Hinshelwood, and Arrhenius parameters. Carbon, submitted for publication.